Morphological and functional properties of the conducting human airways investigated by *in vivo* CT and *in vitro* MRI

Tristan Van de Moortele[1], Christine H. Wendt[2], Filippo Coletti[1]

[1]Department of Aerospace Engineering & Mechanics, University of Minnesota, Minneapolis, MN
[2]Department of Medicine, VA Medical Center, University of Minnesota, Minneapolis, MN

ABSTRACT

The accurate representation of the human airway anatomy is crucial for understanding and modeling the structure-function relationship in both healthy and diseased lungs. The present knowledge in this area is based on morphometric studies of excised lung casts, partially complemented by *in vivo* studies in which computed tomography (CT) was used on a small number of subjects. In the present study, we analyze CT scans of a cohort of healthy subjects and obtain comprehensive morphometric information down to the seventh generation of bronchial branching, including airway diameter, length, branching angle, and rotation angle. While some of the geometrical parameters (such as the child-to-parent branch diameter ratio) are found to be in line with accepted values, for others (such as the branch length-to-diameter ratio) our findings challenge the common assumptions. We also evaluate several metrics of self-similarity, including the fractal dimension of the airway tree. Additionally, we use phase-contrast magnetic resonance imaging (MRI) to obtain the volumetric flow field in the 3D printed airway model of one of the subjects during steady inhalation. This is used to relate structural and functional parameters and, in particular, to close the power-law relationship between branch flow rate and diameter. The diameter exponent is found to be significantly lower than in the usually assumed Poiseuille regime, which we attribute to the strong secondary (i.e. transverse) velocity component. The strength of the secondary velocity with respect to the axial component exceeds the levels found in idealized airway models, and persists within the first seven generations.

Key words: airway morphometry, structure-function relationship, computed tomography, magnetic resonance imaging.

New and noteworthy: We perform a comprehensive CT-based study of the conductive airway morphology in normal human subjects, including branch diameter, length, and mutual angles. We find significant departure from classic homothetic relationships. We also carry out MRI measurements of the 3D inspiratory flow in an anatomy-based model, and directly assess structure-function relationships which have so far been assumed. We find that strong secondary flows (i.e. transverse velocity components) persist through the first seven generations of bronchial branching.

The structure of the human lungs, in particular of the airway tree, and its relation to the pulmonary function have been the subject of intense research efforts. The geometric properties of the bronchi determine important physiological parameters such as the resistance of the conducting airways [19], [60]. These in turn influence gas mixing along with the transport and deposition of particles, and thus the response to the inhalation of both harmful and therapeutic substances [38], [39].

The understanding and modeling of the bronchial structure has often been based on classic morphometric studies [24], [25], [66], [80]. The latter have identified, especially for the dichotomously bifurcating conducting airways, common proportions in terms of, e.g., branch length-to-diameter ratio and child-to-parent branch diameter ratio. The consistency of such proportions beyond the inter- and intra-subject variability indicates that the bronchial tree has a self-similar structure [58], [81]. It has indeed been remarked that, at least over a certain range of scales, the airway tree displays a fractal architecture [15], [16], [46], [82]. Moreover, the values of the geometric parameters and their ratios suggest a significant degree of optimality of the human lung structure. For example, the child-to-parent branch diameter ratio (or homothety ratio) was found to closely approximate $2^{(-1/3)}$ [80], which minimizes air flow resistance and entropy production [55], [83], [85]. The structure of a self-similar tree is typically described by its fractal dimension (d_f), although several practical definitions exist which are analogous to each other only for simple mathematical constructs. The formal definition relates to the Hausdorff dimension, which is closely related to the box-counting dimension (d_b) used in several biological settings including imaging of lung tissues [42]. Other metrics of self-similarity can be defined based on widely used physiological relationships. Murray [55] first pointed out that, assuming the flow in a branch or vessel is described by the Poiseuille's solution (valid for fully developed laminar flow in a circular tube), then the optimum flow that minimizes dissipation while maintaining biological viability is obtained for:

$$Q = CD^3 \tag{1}$$

where Q is the volumetric flow rate and C is a constant that depends on the organ and the fluid in question. It was later pointed out that the diameter exponent is regime-dependent, i.e. $Q = CD^n$, with n = 3 for laminar flow and n = 2.333 for turbulent flow [76]. Assuming the branch geometry does not vary significantly while the fluid flows and that the flow regime does not change along the bifurcation, continuity requires:

$$D_{par}^m = D_{min}^m + D_{maj}^m \tag{2}$$

with m = n. To date, n has not been directly evaluated in airways, due to the difficulty of performing detailed 3D flow measurements either *in vivo*, *ex vivo*, or even *in vitro*. On the other hand, m was estimated from morphometry to be between 2.7 and 3.0 in various mammal vascular beds [33] and around 3.0 in the bronchial tree [26], [35], [45]. In general, m was found to be fairly consistent along the tree, which Mandelbrot [47] saw as proof that biological trees possess a fractal structure.

The symmetric Weibel model and the asymmetric Horsfield model have been adopted in numerous studies investigating respiratory fluid dynamics, both experimentally [14], [28], [29], [70] and numerically [6], [10], [51], [59], [77], [89]. These models possess great simplicity and allow focusing on fundamental aspects of the air and particle transport that transcend anatomical variability, while enabling direct comparison among studies. On the other hand, they are based on a small number of airway casts, on which accurate and repeatable geometry measurements are difficult [69], [75]. Moreover, different excision and casting techniques may affect the morphometric results [75]. In the last decades, advances in medical imaging, especially Computed Tomography (CT), have enabled the *in vivo* measurement of the geometry of the central conducting airways in normal patients, providing information on bronchial length,

diameter and 3D bifurcation angles. Still, most of these studies only considered one subject [69], [74], with only one study considering ten subjects [54]. Moreover, many studies have focused exclusively on airway lumen and wall thickness because of their relevance to obstructive lung disease [1], [20], [56]. Finally, morphometric parameters are often reported only as averages across all reconstructed branches. Generation-by-generation information on the airway geometry is desirable, especially considering the large changes in air flow regimes expected at different generations [38], [18], [60].

Besides the insight on lung and airway structure, CT also provides significant functional information, especially using multi-detector CT (MDCT) [21], [22]. The *in vivo* structural and functional information from medical imaging can be coupled with fluid and solid mechanics analysis to provide information on lobar ventilation, detailed airflow patterns, particle transport and deposition, and lung mechanics [8], [41], [44], [53], [87], [88]. Significant advances have come from computational fluid dynamics (CFD) thanks to efficient numerical techniques and the steadily increasing computer power, and have allowed the investigation of the detailed air flow fields in anatomically accurate, subject-specific geometries [7], [38], [43], [73], [90]. Yet, the complexities of the respiratory flow, which features separation, recirculation, vortical structures, and laminar-to-turbulent transition, requires thorough experimental validation. Experimental studies in realistic geometries are scarce, partly because laser flow imaging (the most used approach in experimental fluid dynamics) is complicated by the difficult optical access through the complex airway geometry. Therefore, investigations of this type, e.g. using Particle Image Velocimetry (PIV), have been limited to the flow through one or two successive bifurcations in transparent airway casts [17], [71]. On the other hand, Magnetic Resonance Imaging (MRI), used in phase-contrast modality, allows reconstructing the three-dimensional velocity field without the need of optical access [11], [61]. de Rochefort et al. [9] used this technique to image the velocity field along selected slices of the air volume up to the second branching generation. Banko et al. [2], [3] imaged the full 3D flow field in the upper and central airways of a subject-specific 3D printed model applying both steady inhalation and oscillatory ventilation. These studies revealed strong vortical motions, with significant velocity components along planes perpendicular to the mean flow direction (so-called secondary flows). The latter were more intense than in idealized Weibel-type models at similar flow rates [29]. A limitation in the studies of Banko et al. was represented by the simplistic boundary conditions applied at the distal branches, in that the five pulmonary lobes received equal flow rates. In general, past investigations that detailed the airflow field in subject-specific geometries rarely made a direct connection between those and the structural/anatomical features of the airway tree - a lack which we aim to help filling.

The present study is focused on the structural and functional features of the human central airways, specifically in terms of bronchial geometry and airflow features during inhalation. We investigate the airway tree structure and lobar ventilation obtained by CT from a cohort of subjects with normal lung function, and explore the detailed flow distribution for a representative case via *in vitro* phase-contrast MRI in a 3D printed model. Our specific goals are to: (i) extend and complement the available data sets of *in vivo* morphometric measurements of the human airways; (ii) directly evaluate metrics of self-similarity which are often used in models of the bronchial tree; and (iii) analyze the inspiratory flow field, specifically as compared to functional properties of simplified models.

METHODS

Morphometry and lobar ventilation from CT scans

This study was approved by the University of Minnesota Institutional Review Board (IRB# 1410E54644). We examined scans at full inspiration (total lung capacity, TLC) and at the end of a normal expiration (functional residual capacity, FRC) in 36 subjects within the cohort of the COPDGene study [67]. The subjects are life-long nonsmokers with normal lung function and no history of lung disease. The mean subject age was 64, ranging from 50 to 79 years old. The three-dimensional images were acquired using MDCT (see Regan et al. 2011 [67] for details on the imaging protocol). The image resolution was dependent on both the slice thickness, which ranged from 0.5 to 0.75 mm, and the in-plane pixel size, which was determined by the field of view. The image voxel size was nearly isotropic and had a mean value of 0.3 mm^3 [79].

In order to extract the airway morphometry, the inspiratory CT scans were segmented and converted to stereolithography files, representing the surface of the bronchial tree (Fig. 1). The latter was smoothed globally using the weighted Laplacian smoothing algorithm in Magics (Materialise, Leuven, Belgium), which filtered spurious edges caused by limited spatial resolution. The software also allowed centerline extraction through a semi-automatic process, which typically results in deviations below one voxel from the true centerline, and compares favorably to other software platforms [68]. The terminal branches were trimmed along planes nearly normal to the airway centerline. Depending on location and orientation, airways of diameter larger than about 0.6 mm were identified, corresponding to distal ends of bronchi up to the 5th to 15th generation, depending on the path. The present analysis extends down to the 7th generation. Figure 2 shows the number of reconstructed bronchial branches at each generation G_N, where the subscript N indicates the generation number. We follow Weibel ordering and start labeling the airways from the trachea (G_0) and continue downward, labeling branches as belonging to a further generation after each bifurcation. By comparison with the expected number of 2^N branches at each generation (assuming dichotomous bifurcations), the count suggests that most branches down to the 6th generation were captured. The number of identified branches at the 7th generation was still substantial, although the large fraction of branches too small to be accurately reconstructed may affect the statistical results at that generation.

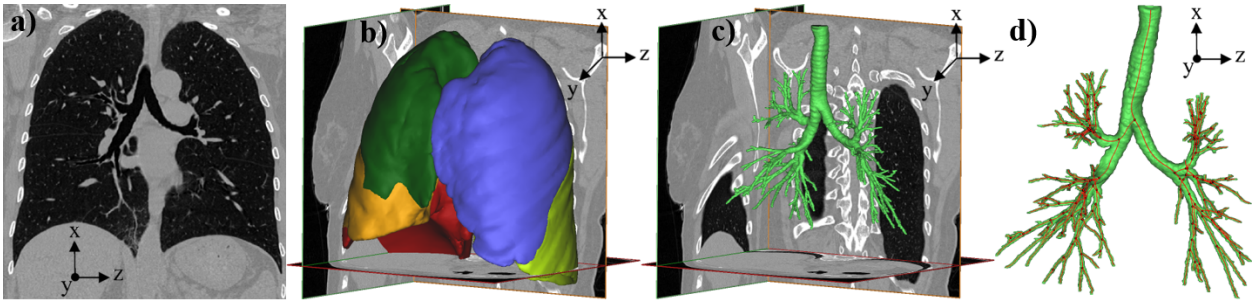

Fig. 1 Segmentation process of CT images: (a) single slice of a CT scan; (b) segmented lobar volumes; (c) segmented bronchial tree air volume; (d) centerline calculated from bronchial tree segmentation. In panel (b), the Right Upper Lobe is dark green, the Right Middle Lobe is orange, the Right Lower Lobe is red, the Left Upper Lobe is blue, and the Left Lower Lobe is light green.

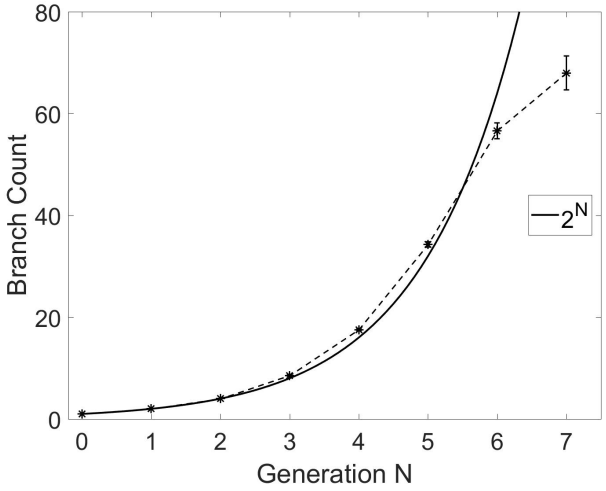

Fig. 2 Branch count per generation, averaged over all cases. Error bars reported in standard error (for a sample size of 36 subjects). The continuous line indicates the theoretical number of branches in a dichotomous tree.

At each reconstructed airway branch and bifurcation, we consider the following geometric definitions (see Fig. 3):

- The airway length L is defined as the distance between the bifurcation points

- The diameter D of each branch is the average over the central 50% of the branch length.

- At each bifurcation, the minor/major branch is defined as the branch with the smaller/larger diameter.

- The branching angle θ is defined as the angle between the forward directions of the parent and child branches. Forward directions for each branch are taken along straight lines joining successive bifurcation points. Compared to taking the local centerline tangent at the bifurcation point, this choice was found to be less sensitive to possible wiggling of the centerline.

- The rotation angle ϕ is defined as the angle between the plane containing the parent branch and its sibling and the plane containing the child branches.

- The non-planarity angle δ is defined as the angle between the parent branch and the plane containing the child branches.

Inspiratory and expiratory scans were compared for each subject in order to assess the lobar ventilation needed to impose appropriate boundary conditions in the MRI flow measurements. For both sets of scans, the five lobes were segmented and separated by identifying fissure lines on the CT images, and the lobar ventilation was established by assessing lobar volume expansion, assuming the tissue volume was conserved [8], [87]. Under this assumption, lobar volume expansion provides a measure of the amount of air inhaled by each lobe, and therefore the fraction of the total inhaled volume [87]. These fractions are to be used in the flow experiments to impose corresponding outflow boundary condition to each lobe (see

section *Inspiratory flow measurements by MRI velocimetry*). Fig. 4 shows the measured lobar ventilation distribution.

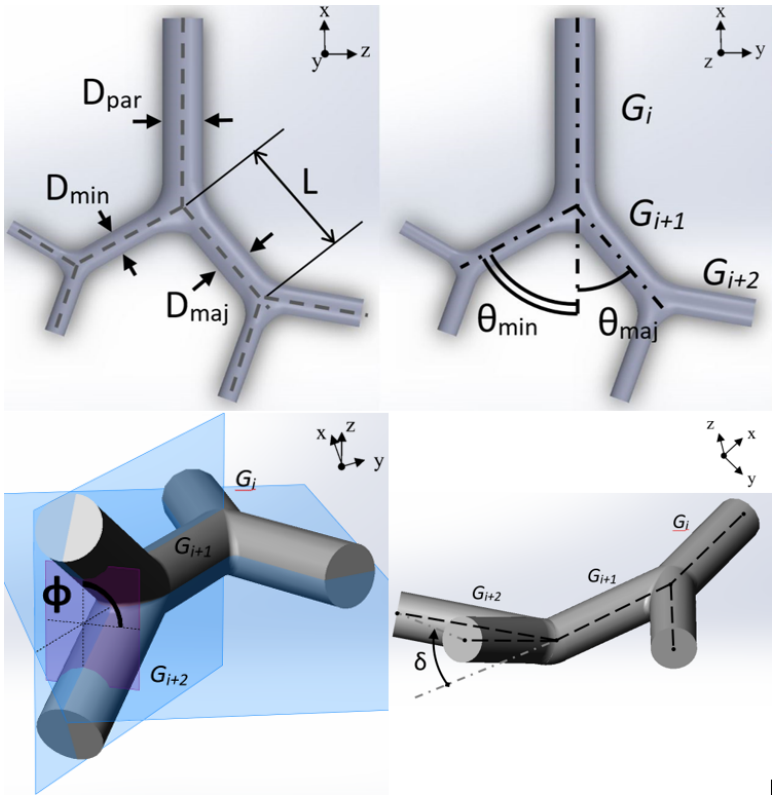

Fig. 3 Schematics illustrating the various geometric parameters considered in the study.

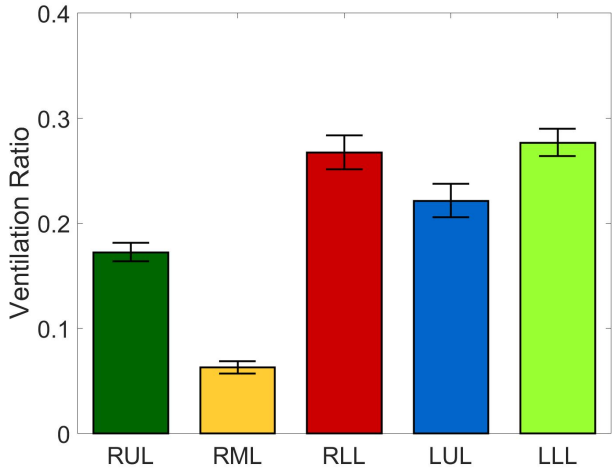

Fig. 4 Lobar ventilation ratios, averaged over all cases. RUL – Right Upper Lobe, RML – Right Middle Lobe, RLL – Right Lower Lobe, LUL – Left Upper Lobe, LLL – Left Lower Lobe. The bars corresponding to each lobe are colored following the color code in Fig. 1(b). Error bars reported in standard error (for a sample size of 36 subjects).

Metrics of self-similarity

We evaluated the degree of airway self-similarity from both the structural and functional standpoint. Several existing structural and functional models and analysis of the airways and other biological trees are based on the assumption, implicit or explicit, that the diameter exponents m and n are equal [31], [36], [45]. The present CT-based airway geometry data allow us to calculate m by solving numerically Eq. 2 at each bifurcation. Moreover, the MRI-based flow data allow us to evaluate n directly from Eq. 1.

The asymmetry at the dichotomous bifurcations, and the consequent flow split, has also been regarded as systematic. Specifically, one can define the flow-dividing ratio *r* as the ratio of flow in the child branch receiving the smaller flow to that in the parent branch:

$$Q_{min} = rQ_{par} \tag{3}$$

from which it follows $Q_{maj} = (1 - r)Q_{par}$. Assuming a constant value of *r* throughout the branch results in a log-normal distribution of the flow rate at the terminal branches of the tree [15], [65]. As with the diameter exponent in Eq. 1, to date it has not been possible to measure *r* directly, and this has rather been deduced from airway morphometry and assuming m = n, i.e.:

$$D_{min} = D_{par} * r^{1/n} \tag{4}$$

Here we use the flow rates directly measured by MRI to calculate *r* from Eq. 3.

To explore the fractal nature of the bronchial tree, we calculate the box-counting dimension d_b from the volumetric reconstruction of the airways of each subject. An isotropic 3D Cartesian grid is superimposed to the segmented bronchial structure and, for a given size Δ of the grid, the number of cubical boxes NB(Δ) needed to cover the whole structure is counted. In the case of a pure fractal set of dimension d_f the number of boxes would follow a power law $NB(\Delta) \sim \Delta^{-df}$. In real systems this relation only holds in a restricted range of scales between a large- and a small-scale cutoff. We define a local exponent as the logarithmic slope:

$$d_b = -\frac{d\{\ln[NB(\Delta)]\}}{d\{\ln(\Delta)\}} \tag{5}$$

and calculate the box counting dimension as a fit over the range for which such slope is approximately constant. Here the most refined grid we use has $(625)^3$ voxels; denser grids have boxes smaller than the smallest reconstructed airways and therefore do not extend the scaling range. Figure 5 shows the box count NB(Δ) as a function of box size Δ for a subset of the considered subjects, indicating strong self-similarity over more than one decade.

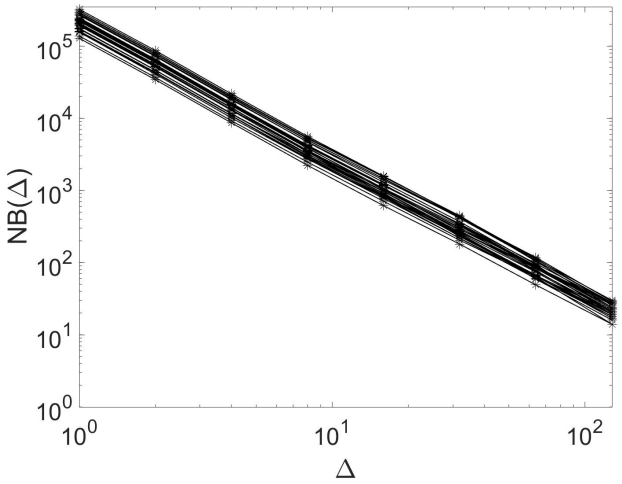

Fig. 5 Three-dimensional box counting of the airway tree: log-log plot of the box size Δ vs the box count NB, for a subset of the considered subjects. Here Δ has units of voxels.

Inspiratory flow measurements by MRI velocimetry

In order to assess the details of the inspiratory flow field through the bronchial tree, the airway tree of one subject case was used to build a 0.85 : 1 physical model, which was then employed for MRI velocimetry. The selected subject was representative of the cohort in that it had morphometric features close to the mean of the distribution for all geometric parameters. A 2.5 mm thick solid was created from the inspiratory airway surface using the software 3-Matics (Materialise, Leuven, Belgium). A five-cavity enclosure was then built around it using the software SolidWorks (Mountain View, CA), creating a one-piece model (Fig. 6). The five cavities were used to collect the flow from the terminal bronchi of each lobe, in a similar fashion as in Banko et al. [2], [3]. The model was 3D printed at the W.M. Keck Center (University of Texas El Paso, TX) using Watershed XC 11122. The high resolution print (25 μm layer thickness) guaranteed that the inner walls of the model were hydrodynamically smooth.

Water was used as the working fluid, with the addition of copper sulfate at 0.06 mol/L in order to maximize the MRI signal without changing the fluid properties. While MRI velocimetry has been performed with gases such as ^{3}He and SF_6 [9], [12], water offers much higher signal than unpolarized gas at much shorter scan times, while hyperpolarized gases can become unpolarized during use [12]. The flow in a rigid airway model is completely characterized by the Reynolds and Womersley numbers [30]; in the present case in which steady inhalation is considered, only the former needs to be matched. Therefore, dynamic similarity with air flow is achieved by adjusting the water flow velocity to compensate for its lower kinematic viscosity.

The MRI experiments were carried out at the University of Minnesota Center for Magnetic Resonance Research, and the procedure was similar to what described in our recent study of the flow in a Weibel-type model [29]. The flow was driven by a centrifugal pump (TE-6-MD-SC, Little Giant) that circulated the fluid from a reservoir through the model and back to the reservoir, which were connected via plastic tubing 2.5 cm in diameter. The volume flow rate was regulated by a digital flow controller (LCR-5LPM-D, Alicat Scientific Inc.) with approximately 2% uncertainty. The flow was carried through tubing with a diameter of 25mm,

and entered the trachea through a separately 3D printed piece that smoothly connected the two, preventing any geometrical step from producing inlet flow disturbances. Each plenum had a separate outlet, with needle valves to adjust their respective return flow rates. These were measured with a transonic flow meter (Transonic TS410 Tubing Module and Transonic ME-6PXL clamp-on flow probe) and set to match the subject-specific lobar ventilation obtained by the inspiratory and expiratory CT scans. These lobar ventilation fractions are very similar to the cohort-averaged values reported in Fig. 4. All components and bolts were made of plastic to be fully MRI-compatible. The inlet flow rate was 1.6 L/min, which is equivalent (for the same Reynolds number) to about 22.5 L/min of air. The inlet Reynolds number at the trachea, defined as:

$$Re_0 = \frac{U_0 D_0}{\nu} \tag{6}$$

was about 1750, typical of normal breathing conditions [60]. Here U_0 and D_0 are, respectively, the bulk velocity and the hydraulic diameter at the uppermost reconstructed end of the trachea. A 3 Tesla Siemens whole-body scanner was used, with the airway model inserted in a transmit-and-receive radio-frequency coil commonly used for human head imaging. Velocity data were obtained using the method described by Elkins et al. [12], with the signaling and data acquisition sequence from Markl. et al. [48]. The main scan parameters were: repetition time of 34.4 ms, echo time of 8.6 ms, 35 degrees flip angle, and velocity encoding value of 600 mm/s. Three-dimensional velocities were obtained on a uniform Cartesian grid at a resolution of 0.6 mm in all spatial directions. Four successive scans were acquired and averaged to increase accuracy. The expected uncertainty was calculated following Pelc et al. [62], and ranged between 4.8% and 6.3% of U_0 depending on the location.

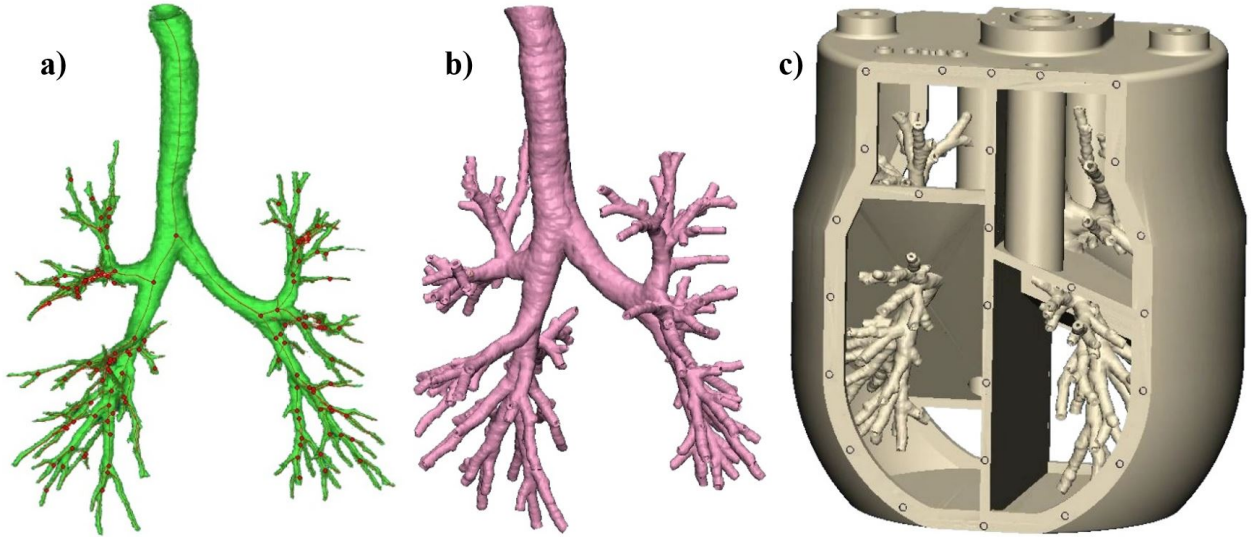

Fig. 6 (a) segmented bronchial tree air volume; (b) thickened and hollowed bronchial tree; (c) CAD rendering of the flow model to be 3D printed.

Our flow analysis is focused on two main quantities: the volumetric flow rate through each branch, and the magnitude of the secondary flows (defined by the velocity components

perpendicular to the branch axis). Considering a branch cross-section of area A perpendicular to the streamwise flow direction **a** (illustrated in Figure 7), the volumetric flow rate is defined as:

$$Q = \int U_{ax} dA \tag{7}$$

where U_{ax} is the velocity component in direction **a**, while U_{sec} lies on the plane of the cross-section. A rigorous definition of the axial direction is necessary. In simple tubular networks this is identical to the geometric axis of each branch, which coincides with the airway centerline. In realistic bronchial trees the geometric centerline may not be exactly aligned with the mean flow direction in the branch, due to the complexity of the airway morphology and the flow trajectory. Therefore, we apply conservation of mass to establish the axial direction as the direction along which the flow is aligned. Specifically, for each branch we run an optimization routine to find the cross-section orientation that minimizes the average in-plane velocity (which at rigor should be zero). The local centerline direction is adopted as first guess and the cross-section orientation is varied incrementally until the residual in-plane velocity is below 1% of the out-of-plane component. Finally, to calculate Q and U_{sec}, multiple cross-sections spaced by one voxel size (0.6 mm) are considered and averaged over the central 50% of the length of each branch.

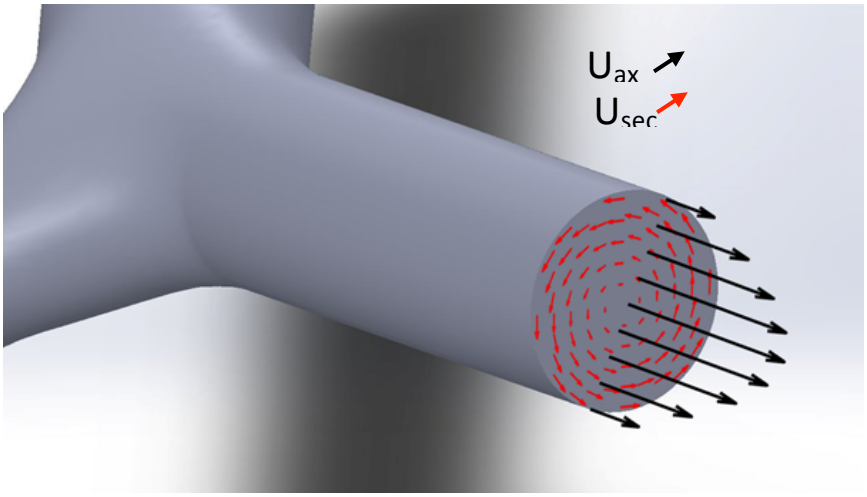

Fig. 7 Diagram illustrating branch-axial velocity U_{ax} and the cross-sectional plane velocity U_{sec} in a branch.

RESULTS

Airway morphometry

The tree-averaged morphometric results are summarized in Tab. 1. In the following we present each of them in some detail.

Parameter	**Mean ± SD**
Number of reconstructed branches per subject	192 ± 31
D/D_0	0.26 ± 0.04
L/D_0	0.76 ± 0.08
H	0.79 ± 0.02
h_{min}	0.73 ± 0.02
h_{maj}	0.85 ± 0.02
D_{min}/D_{maj}	0.86 ± 0.01
L_{min}/L_{maj}	2.0 ± 0.24
L/D	3.4 ± 0.3
$(L/D)_{min}$	4.3 ± 0.4
$(L/D)_{maj}$	2.8 ± 0.4
θ [°]	66 ± 3
θ_{min} [°]	36 ± 2
θ_{maj} [°]	31 ± 2
ϕ [°]	54 ± 2
δ [°]	7.8 ± 0.8

Table 1 Morphometric parameter results (mean ± standard deviation). D: branch diameter; L: branch length; h: child-to-parent diameter ratio; θ: branching angle, ϕ: rotation angle, δ: non-planarity angle

Figure 8 shows the airway diameter (normalized by the value at the trachea D0), as a function of the branching generation. In this and in the following plots the error bars represent +/- standard error (for all branches at each generation and for all patients), while in the table and in the text we report mean +/- standard deviation in order to highlight the statistical spread. The semi-log plot in Fig. 8a highlights the expected exponential decay with branching generation [84], which is the consequence of an approximately constant value of the child-to-parent diameter ratio h. The theoretical trend obtained assuming $h = 0.5(1/3) \approx 0.79$ [80] is also indicated, yielding excellent agreement. This is confirmed also by explicitly plotting h as function of generations. The overall average of 0.79 ± 0.02 is consistent with published values [52], [54], [74]. The homothety ratio appears to be remarkably consistent along the conducting airways, in contrast with the increasing trend found by Montaudon et al. [54].

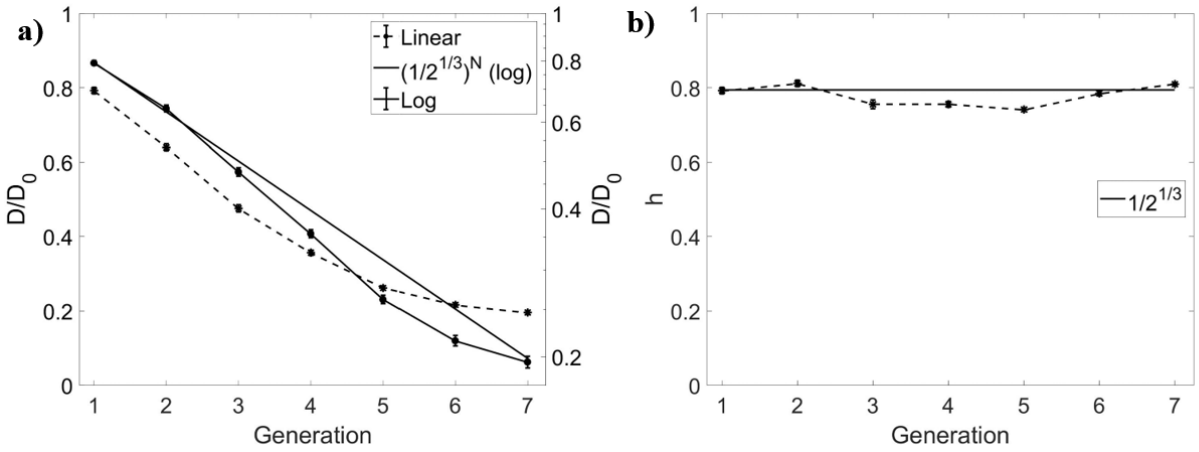

Fig. 8 (a) D/D_0 vs generation; (b) homothety ratio h vs generation. Error bars reported in standard error. In both panels, the straight continuous line indicates the theoretical trend with $h = 2^{(-1/3)}$. In panel (a), D/D_0 is plotted in both linear scale (dashed line, left axis) and logarithmic scale (continuous line, right axis).

The evolution of the normalized airway length L/D_0 along successive generations is plotted in Fig. 9a. After a quick drop of the length of the bronchi in the first three generations, the values reach an apparent plateau, although this cannot be firmly concluded from the present data limited to G_7. When considering the branch aspect ratio L/D (Fig. 9b), large fluctuations are found. In addition, the mean value over all branches is significantly larger than the value of ~3 generally quoted [52], [64], [69], [80], but the standard deviation is very large and consistent with the measurements of Sauret et al. [69] and Tawhai et al. [74]. Despite the scatter, a markedly non-monotonic trend is visible, with the branches becoming shorter (relatively to their diameter) at G_2 and G_3 and recovering length deeper in the tree, where the relatively long and numerous branches at G_5-G_7 increase substantially the mean L/D value. A similar trend was visible in the original data of Weibel [80], with a minimum of L/D for G_3, but to our best knowledge it has not been reported since then. In reanalyzing Raabe's data, Philips & Kaye [64] did remark that, with decreasing diameter, the airway length decreased less than what proportionality would imply.

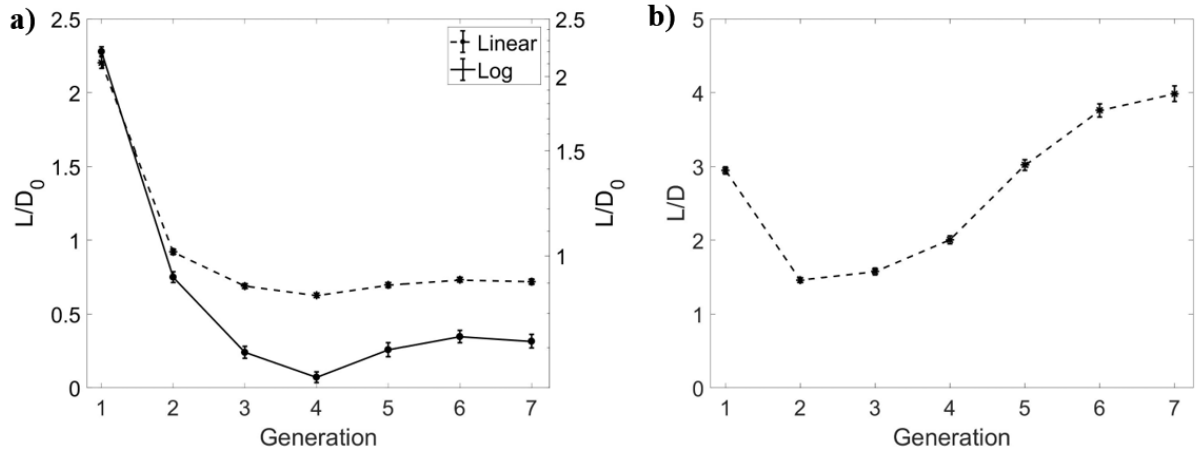

Fig. 9 (a) L/D_0 vs generation; (b) L/D vs generation. Error bars reported in standard error. Notice that, in panel (a), L/D_0 is plotted in both linear (left axis) and logarithmic (right axis) scales.

Figure 10 plots the branching angle θ, the rotation angle ϕ, and the non-planarity angle δ, as a function of the generation number. The average value of θ = 66° ± 3° is consistent with the published range [23], [63], [69], [74]. Previous measurements based on casts showed contradictory trends in terms of variation of the branching angle along the airway tree, with Phalen et al. [63] and Horsfield & Cumming [24] reporting decreasing and increasing θ with deeper generations, respectively. As previously pointed out, obtaining accurate measurements of airway angles from casts is a complicated operation [75]. Here we find that θ, over the considered range of generations, follows a decreasing trend with more distal airways. The rotation angle ϕ is typically assumed equal to 90° in analytical and computational models [10], [36], [49], according to the large angles reported by morphometric reports from casts [27]. The *in vivo* measurements of Sauret et al. [69] and Tawhai et al. [74] found average values of 79° and 76° degrees, respectively; both considered only one subject. We find a significantly lower average of ϕ = 54° ± 2°. The rotation angle is in fact much smaller for the bifurcations leading to the lobar bronchi (consistent with the fact that lung imaging of coronal sections typical capture several proximal branches), and it is then about 55° in the further generations up to G_7. The non-planarity angle δ, which is usually assumed null, was measured here for the first time. We confirm that this angle takes small values, according to physiological principles of wiring cost minimization in biological trees [34].

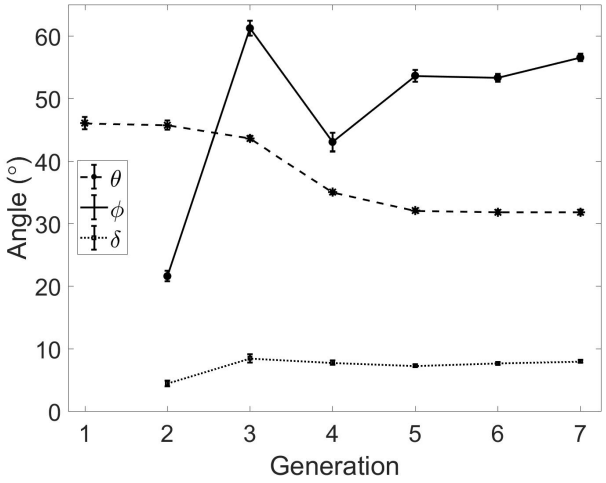

Fig. 10 Branching angle θ, rotation angle ϕ, and the non-planarity angle δ vs generation. Error bars reported in standard error.

Previous morphometric studies indicated significant asymmetry in the bronchial tree [24]. Here we address the differences between sibling airways in terms of diameter, length, and branching angle. Figure 11a displays the ratio D_{min}/D_{maj}, bound to be smaller than one. The average across all reconstructed generations is 0.86 ± 0.01, in the range of published data [63], [74], [80], and the ratio is also fairly consistent across the different generations. Consequently, the values of h calculated for the minor and major child branch are also consistent along the

airway tree, and have averages of 0.73 ± 0.02 and 0.85 ± 0.02, respectively; these too are within the published ranges [64], [74]. On the other hand, the ratio L_{min}/L_{maj} (the length of the smaller-diameter child divided by the length of the larger-diameter child) show a surprising behavior. The latter appears to be consistently larger than unity, with an average of 2.0 ± 0.24. The fact that larger siblings have shorter length is seemingly against the idea of an L/D proportion, which is instead widely accepted. However, a closer look at previously reported data shows that our finding is consistent with the acknowledged asymmetry of the bronchial tree. Indeed the ratio L/D for major child branches was consistently reported to be smaller than L/D for minor branches [64], [74]. For example, Tawhai et al. [74] reported mean values of $(L/D)_{maj} = 2.48$ and $(L/D)_{min} = 3.63$. Since they also reported $D_{min}/D_{maj} = 0.85$, one deduces from their data that $L_{min} > L_{maj}$. The distribution of L_{min}/L_{maj} has a log-normal behavior (Fig. 11b): although the most likely configuration features siblings of comparable length, instances of one child branch being several times longer than the other are not uncommon. The fact that the larger sibling tends to be systematically shorter is confirmed by the scatter plot in Fig. 11c, which indicates a negative correlation between D_{min}/D_{maj} and L_{min}/L_{maj}.

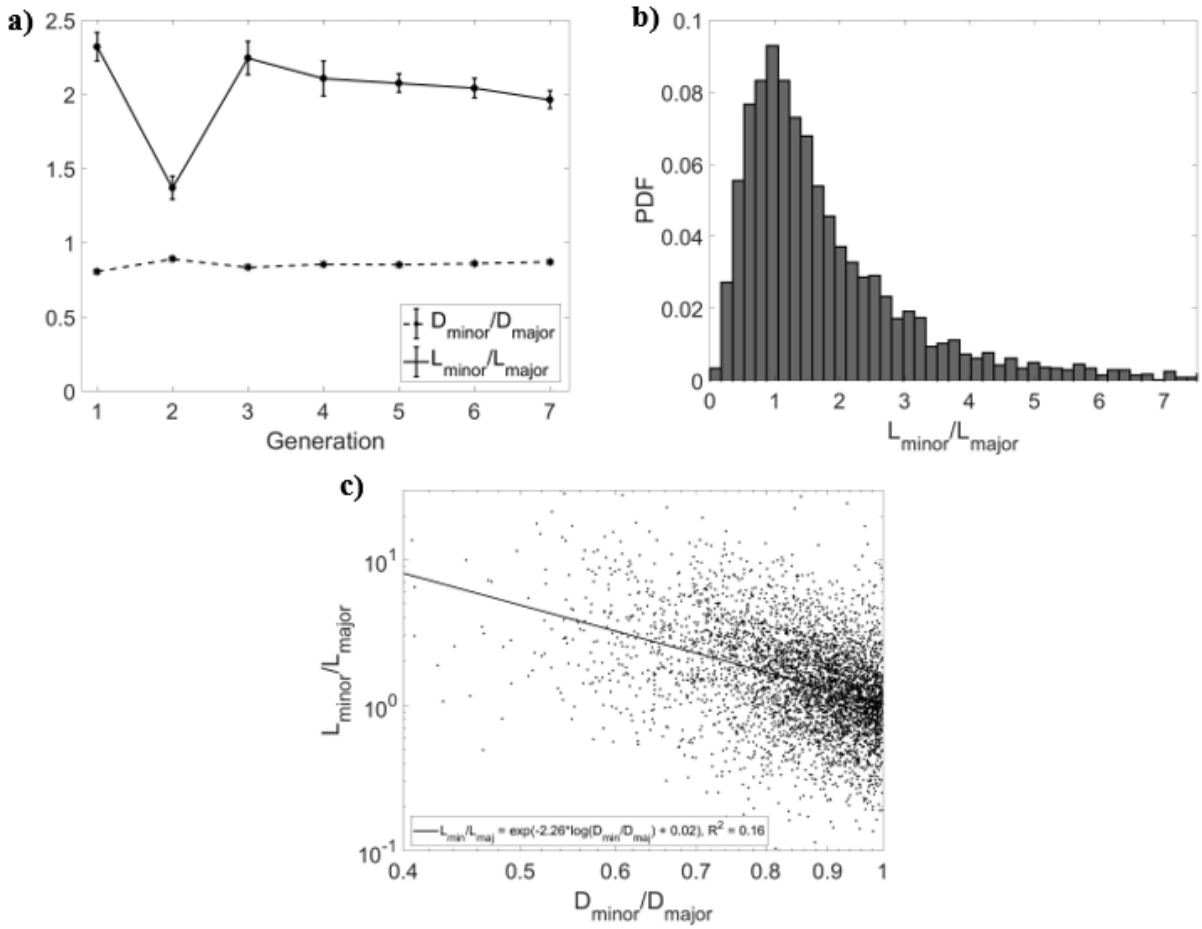

Fig. 11 (a) D_{min}/D_{maj} and L_{min}/L_{maj} vs generation; (b) probability distribution function of L_{min}/L_{maj}; (c) scatter of D_{min}/D_{maj} vs L_{min}/L_{maj}, with linear least-square-fit line and showing fit equation and R^2 coefficient ($p < 0.001$). Error bars reported in standard error.

In Figure 12 we show the branching angles made by the major and minor child airways at different generations. Except for G_2, the larger siblings appear to make a significantly smaller angle than the smaller ones. Phalen et al. [63] reported that branching angles in humans were fairly symmetric compared to other animals. However, their analysis (based on Raabe's data) does show consistently larger angles, by 10 degrees or more, for minor branches than for major branches. We find that in 49% of sibling pairs the minor sibling angle is at least 10 degrees larger than the major sibling angle.

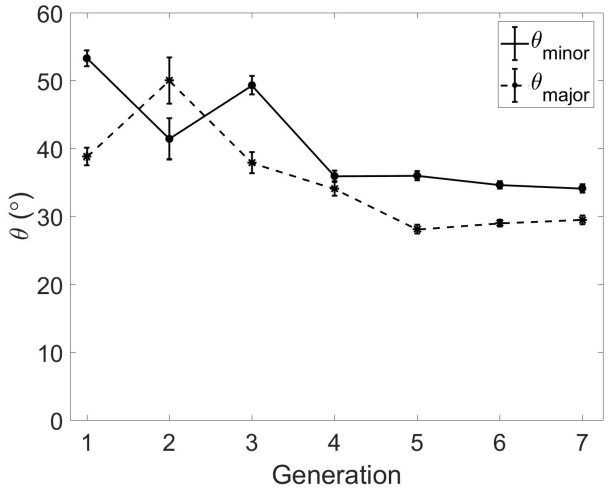

Fig. 12 Branching angles θ_{min} and θ_{maj} vs generation. Error bars reported in standard error.

Diameter exponent and flow-splitting ratio

In figure 13 we directly verify the validity of $Q = CD^n$ using the CT-reconstructed airway diameters and the respective flow rates measured by MRI velocimetry, showing the probability distribution of n. Both flow rate and diameter are normalized by their value at the trachea, Q_0 and D_0 respectively. A best fit in a log-log scatter plot well represents the data, supporting the assumption that n is fairly constant along the airway tree. The least-square fit value of 2.36 (close to the mathematical mean of 2.4) is significantly smaller than what previously reported (e.g. 2.9 by Horsfield & Thurlback [26], and 3.0 by Kitaoka & Suki [35]). Previously reported values, however, have always been for the exponent m in Eq. 2 rather than for n.

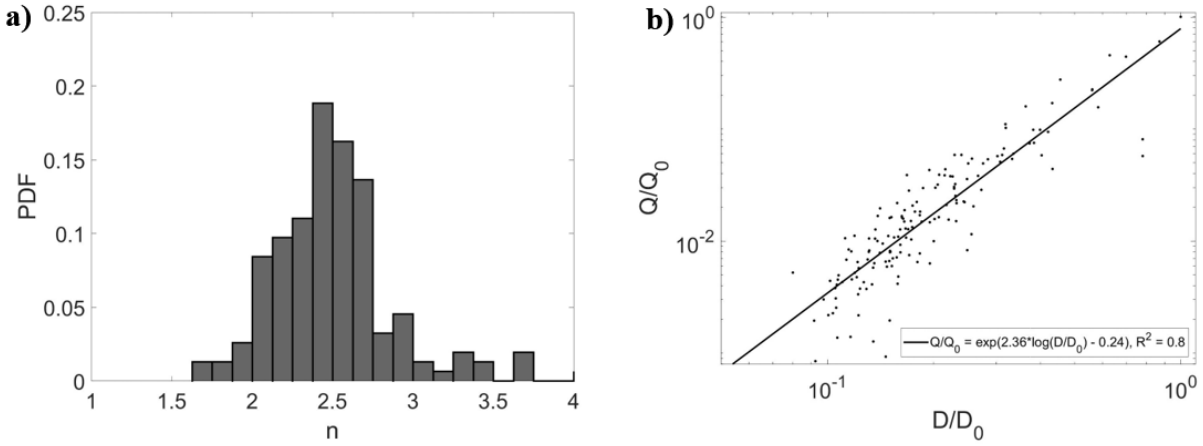

Fig. 13 (a) probability distribution function of n; (b) log-log scatter of D/D_0 vs Q/Q_0, superimposed with linear least-square-fit line and showing fit equation and R^2 coefficient ($p < 0.001$).

In Figure 14a we show the probability distribution of m calculated by applying Eq. 3 to the reconstructed bronchial trees. This resembles what is reported by Horsfield & Thurlbeck [26] and Kitaoka & Suki [35] (using Raabe's data) and appears to follow a log-normal behavior. Figure 14b depicts the variation of m with the generation number, and suggests a decreasing trend along the airway tree. Since Re decreases at each generation, this would appear to contradict the general idea that the exponent becomes lower for fully laminar flow [76], [26]. However, one should keep in mind that m is only an approximation for n. Also, the canonical values of 2.333 for turbulent and 3 for laminar flow assume fully developed regime, which is never achieved in the airways, as we also discuss in the next section.

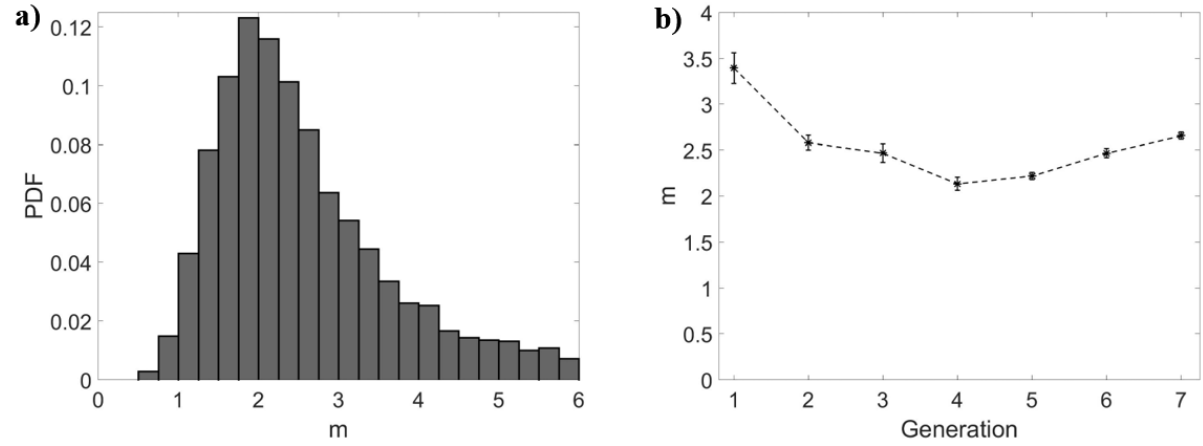

Fig. 14 (a) probability distribution function of m; (b) m vs generation. Error bars reported in standard error.

Knowing the flow rate at each bifurcation, we can directly calculate the flow-dividing ratio *r* (Eq. 3), which is an important parameter in asymmetric airway flow models [35], [36], [45]. The average values of *r* measured by MRI is 0.32, but there is significant scatter and no clear trend with generation number. This is consistent with the assumption of Kitaoka & Suki [35], who proposed a tree model with *r* uniformly distributed between 0.2 and 0.5. On the other

hand, Majumdar et al. [45] assumed constant values for *r* across their tree model. If one uses Eq. 4 to calculate an average value, n = 2.4 and $h_{min} = D_{min}/D_{par} = 0.73$ (see Tab. 1) yield $r = 0.47$. Assuming the usual diameter exponent value of n = 3 instead yields $r = 0.39$.

Fractal dimension

We evaluated the box-counting dimension in two ways. First, we consider the least-square linear fit in the log-log plot (Fig. 5) in the range $\Delta = 2 - 60$. Second, we calculate the local slope from Eq. 5, and take its average value over the same range. The two methods returns box-counting dimension 1.89 and 1.9 respectively. In order to assess the importance of evaluating the fractal dimension on the actual 3D geometry (as opposed to a planar image of it), we project the geometry onto a coronal plane and repeat the box count in 2D using up to $(625)^2$ square elements. This leads to a box-counting dimension of 1.8; the mismatch with the 3D value underlines the need of performing a full volumetric analysis for accurately capturing the fractal dimension of the highly three-dimensional airway tree.

Kamiya & Takahashi [31] reasoned that the fractal dimension d_f (calculated as the box-counting dimension or by similar techniques based on the probability distributions of branch sizes) is related to the (geometric) diameter exponent m by:

$$m = d_f + \alpha \tag{8}$$

where α is the exponent in a power-law relationship between the branch length and the diameter [31], [72]:

$$L = \beta D^{\alpha} \tag{9}$$

α is typically reported to be around 1, consistent with the fact that several airway morphology studies showed fairly constant L/D ratios [66], [80]. Assuming $\alpha = 1$, the values for the fractal dimension and the diameter exponent appear consistent with Eq. 8.

Secondary flows

The flow rate gives a measure of the axial flow velocity in each branch. A complementary metric describing the transport in the airways is represented by the secondary flows, whose intensity is shown in Figure 15. This is evaluated as the magnitude of the secondary velocity component U_{sec} (see Fig. 4) along each branch cross-section, and averaging over the central 50% of the branch length, similarly as for the flow rate calculation. When normalizing by inflow velocity at the trachea, U_0, the secondary flows appear to build up in the first couple of bifurcations and then steadily decrease through the bronchial tree due to the general reduction of the velocity magnitude. On the other hand, when normalizing by the local bulk (i.e. cross-section averaged) axial velocity, U_{ax}, the secondary flow strength peaks at 25% and remains steadily above 17% of the streamwise velocity component. This is larger than the secondary flow strength found in idealized airway models. For example, Isabey & Chang [28] found that the secondary flow

magnitude never exceeded 16% of the axial velocity in a Horsfield-type model, while according to Fresconi & Prasad [14] it did not exceed 10-20% in a Weibel-type model.

DISCUSSION

Cast-based morphometric models of the human airways such as Weibel's and Horsfield's have been invaluable to the lung physiology community. With the availability of accurate *in vivo* measurements of airway geometry via medical imaging [54], [69], it is natural to incorporate those in more realistic representations of the bronchial tree [74]. Beyond the purely anatomical measurements, the transition from the structural to the functional information has been usually based on simplistic assumptions on the nature of the flow, for example fully laminar and developed (Poiseuille) regime [31], [36]. With the advent of advanced computational methods and volumetric velocimetry techniques, it has become possible to reconstruct the full flow field in realistic models

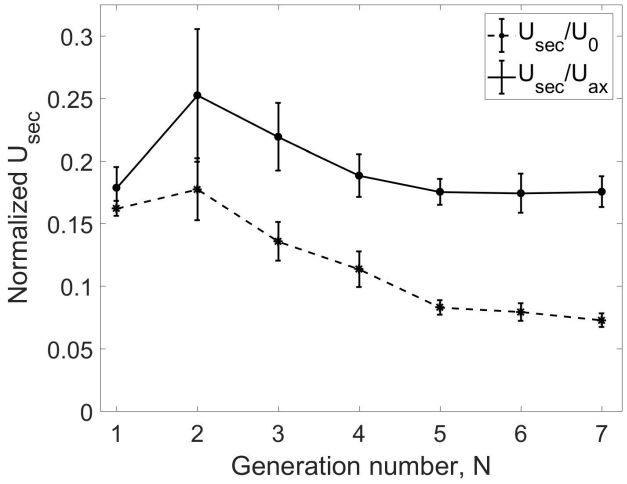

Fig. 15 Secondary velocity magnitude U_{sec} normalized by the bulk tracheal velocity U_0 and the local branch bulk velocity U_{ax} vs generation. Error bars reported in standard error.

across many generations [2], [7], [43], [90], enabling a more accurate definition of the structure-function relationship. In the present study, we have used high-resolution lung CT scans of 36 healthy subjects to determine the anatomical features of their airway tree. We have then created a physical model of one subject's tree, and used it to measure the detailed flow field throughout via phase-contrast MRI, while imposing steady inspiratory flow rate and patient-specific lobar ventilation. We have therefore been able to evaluate classic morphometric features from the cohort, as well as to test widely used structure-function relationships for the central airways. While we had previously used MRI velocimetry to explore the flow pattern in subject-specific airway geometry [2], this is the first time that this technique is used to explore respiratory physiology and to probe structure-function relationships.

Previous morphometric *in vivo* studies have considered only one subject [69], [74], or have measured only selected quantities such as lumen area [54]. From the present cohort we have

reconstructed over 3 thousand branches extending over seven bronchial generations, and measured branch diameter, length, bifurcation angle, rotation angle, and bifurcation planarity, along with several measures of bifurcation asymmetry. We find that several parameters of proportionality show remarkable self-similarity over the investigated generations, while others vary significantly along the tree. Specifically, the homothety ratio is fairly constant and close to the optimal ratio of 0.79 [80]. The length-to-diameter ratio instead varies significantly, being smaller than the usually quoted value of 3 for generations G_2 and G_3, and growing well above such value for further generations. This confirms previous observations that the airway lengths do not get uniformly smaller with further generations at the same pace as diameters do [40], [52]. The change in branch length-to-diameter ratio could have significant impact on the airways resistance. According to Pedley [60], for fixed flow rate and bulk velocity, the pressure drop due to viscous dissipation is proportional to $(\mathrm{Re}\cdot L/D)^{1/2}$ (a relationship shown to be at least qualitatively correct by numerical simulations in idealized models [6]). Our results show that L/D tends to be significantly below the average in upper generations where Re is higher, and vice versa in deeper generations. Therefore, it is possible that realistic bronchial trees (having long airways deeper in the bronchi, where the pressure drop per unit length is smaller) offer lower resistance than equivalent trees of constant L/D = 3. We remark, however, that this argument does not account for other geometric factors that may affect airway resistance (such as the precise bifurcation geometry), nor for the effect of unsteadiness/turbulence at higher Re. The branching angle shows a steadily decreasing trend from about 95° at G_1 to 65° at G_6 and G_7. The rotation angle is significantly smaller than what previously reported, hovering around 55°. The bifurcations are confirmed to be planar, and strongly asymmetric: the minor branch is typically about 20% smaller in diameter than its major sibling, but also significantly longer, and making a somewhat larger angle with the direction of the parent branch. Therefore, although human airways are more symmetric compared to other mammals [63], the present data suggest (as also indicated by several past studies) that systematic asymmetries need to be incorporated in realistic lung models, beyond the simple difference of siblings' diameter. In particular, to our best knowledge, the fact that minor child branches are much longer than major ones had not been reported before; this possibly went unnoticed due to the large variability of L and the limited number of samples considered in past studies. Indeed, most previous morphological reports with relatively large cohorts focused on airway lumen rather than length [54], [79]. This geometric feature of the lungs might have far reaching consequences, potentially impacting the unevenness in flow distribution due to differences in resistance. This awaits to be explored by functional airway models.

Despite the patently fractal nature of the airway structure, direct measurements of the fractal dimension d_f of the airway tree have been sparse and mostly based on cumulative measures of airway branch length, which are strongly dependent on the branch ordering method [57]. The difficulty stems from applying to real systems definitions of d_f which are originally meant to describe mathematical constructs. For vascular systems, which are routinely imaged to great detail by *in vivo* CT using contrast agents, the common approach has been the box-counting method. Using this technique several groups reported d_f around 1.7 for the retina blood vessels [50], and Boxt et al. [5] measured $d_f = 1.62$ for the pulmonary circulation. This approach was followed also by Boser et al. [4] to measure $d_f = 1.83$ in the airway tree by analyzing 2D pictures of casts. We perform the first *in vivo* estimate of the airway fractal dimension using the box-counting method on the fully 3D reconstructed tree, and find a fractal dimension between 1.88 and 1.9. This suggests that, over the scaling range available with the present resolution, the

bronchial tree appears to be more space-filling than typical vascular beds. Moreover, we pointed out how considering only a 2D image of the highly three-dimensional bronchial tree might lead to a somewhat misestimated value.

Another important metric of self-similarity is the diameter exponent n in the flow-diameter relation $Q \sim D^n$, which is often used as a foundation to construct structural and functional tree models [31], [35], [36]. Besides the CT-based diameter, we have exploited the information on the flow rate at each branch obtained by *in vitro* MRI velocimetry to evaluate such exponent, yielding n = 2.36. Previous estimates have all evaluated the exponent indirectly, using solely the geometry, yielding values closer to n = 3, i.e. the optimum value for Poiseuille flow [14]. One could deduce that, over the considered portion of the tree, the flow through the airways is rather turbulent than laminar (n = 2.333 being the optimum for fully developed turbulent flows [58]). However, we do not draw such a conclusion. The Reynolds number (which we directly calculate using the axial velocity at each branch obtained by MRI) rapidly decreases at each generation because of the flow split among successive bifurcations and the reduction in airway diameter. Here at the second generation it is already Re < 1000. Therefore, even if unsteadiness may ensue at the upper generations, turbulence is unlikely to develop in the considered regime. Rather, one should keep in mind that both n = 2.333 and n = 3 represent optimal conditions obtained for fully developed flows - a situation which is never achieved in the relatively short airway branches. The bronchi always see developing flows, with boundary layers growing over their entire length [60]. Moreover, the streamlines do not describe a "parallel flow" (such as the Poiseuille flow), but have a strongly spiraling motion produced by the intense secondary velocities. Therefore, while the flow might be turbulent or at least unsteady in the first few generations depending on the inhalation flow rate [18], [60], even at laminar regimes the inspiratory flow is not well represented by the Poiseuille solution; therefore a departure from n = 3 is expected, and the relatively strong secondary flows contribute to such departure, leading to an n exponent similar to that of turbulent flow. The magnitude of the secondary flow motions is found to be consistently larger than 17% of (and locally it can be as high as) the local axial velocity, significantly more intense than in canonical (Weibel-type or Horsfield-type) models [14], [28]. Importantly, the relative strength of the secondary flow is maintained deep in the bronchial tree. This may have far-reaching consequences for, e.g., the transport of therapeutic and harmful particles, which are highly responsive to vortical motion [38]. To date secondary flows have not been directly incorporated in analytical models of lung structure and function [13], [36], [45]. This class of models typically assumes a flow-diameter relationships and/or straight parallel flow in each branch. Given the relative strength of the secondary flows found in realistic geometries, and the fact that these appear to persist up to at least the 7^{th} generation of branching, we argue that similar models could benefit from incorporating these motions in the flow representation; especially because these motions affect not only pressure drop but also gas mixing and particle transport [14], [37], [90]. The practical implementation (e.g. through empirical corrections) is beyond the scope of this work, but further research in this area is warranted.

The present study has several limitations. The number of considered subjects, while being the largest to date in morphometric studies of this kind, is limited; future studies on larger cohorts should provide more accurate mean values for the geometric parameters. The resolution of the CT scans we used is state-of-the-art, but still limited in terms of the depth of the generations we could resolve. Indeed, the precise values of our G_6 and G_7 estimates are likely affected by the fact that not all branches at those generations could be captured. The respiratory

flow investigation has focused solely on steady inspiration. Several previous studies show that, at low to moderate respiration frequency, the effects of the time-dependent oscillation cycle are indeed minor [89], [14]. In particular, the flow fields in steady and unsteady inspiration agree fairly well, except during the deceleration phase and near flow reversal [38]. Such a regime, in which the viscous forces prevail over the unsteady inertial forces, is characteristic of quite breathing. Also deep inhalation maneuvers associated with aerosol drug delivery are typically considered quasi-steady, as far as the central airways are concerned. In these conditions, we therefore expect features such as the secondary motions to be well reproduced by steady inspiratory experiments. On the other hand, under faster-paced breathing patterns typical of high-frequency ventilation and exercising, the oscillatory flow in the inhalation phase is qualitative different from steady inhalation [3], [17], and therefore the present results cannot be extended to those regimes. The MRI flow measurements were performed on a rigid model, not accounting for any airway compliance. This is common practice in both experimental and numerical studies [38], in keeping with the assumption that the variation of airway length and diameter throughout the first few generations are not large. Computational studies including fluid-structure-interaction indicate that the effect on flow distribution and intensity of secondary flow is moderate [78]. Still, wall motion does have an effect on the flow pattern and even more on the wall shear stresses [86], and its influence shall be investigated more in depth in future functional models. This however remains a challenge due to many unknowns on the mechanical properties of the airway walls [32], which can possibly be addressed with input boundary conditions from 4D CT imaging [88]. The airway model did not include the upper airways, which are expected to have a significant effect on the flow features downstream [43]. Our focus was on the bronchial tree, and the present approach allowed us to isolate the fluid dynamics in it. Accurate reconstructions of the mouth-throat geometry are much less common than central airways (typically obtained by CT), due to the sizeable level of radiation to the head in those type of scans. It is therefore important to investigate structure-function relations that can be applied to the airway geometry directly available from common chest scans. Moreover, the effect of the upper airways would mainly affect G_1 and G_2, while most of our results (including the flow-diameter relation and the relative strength of the secondary flows) apply across the reconstructed generations. MRI measurements have been carried out for only one subject, limiting the statistical power of the findings. The process of generating deep airway models and imposing the appropriate lobar ventilation is elaborate, and the MRI flow measurements are involved. The reported values of secondary flow intensity are indeed consistent with what previously obtained for a different subject using similar methods [2], lending credibility to the present conclusions. In the future, opportunely validated CFD solvers can be used to extend the present study to a much larger cohort. While current CFD allows high-fidelity reconstruction of the 3D airflow in both idealized and realistic airway geometries, this has rarely been used to explore fundamental structure-function relationships [51]. Indeed, once the structural and functional parameters we have investigated (as well as others) are established for healthy lungs, image-based measurements and simulations can be leveraged for timely and non-invasive diagnosis of airways disease and assessment of the disease progression. The morphometric data used for this study is available online at https://www.lib.umn.edu/datamanagement/drum.

ACKNOWLEDGMENTS

We gratefully acknowledge the access to the COPDGene database. We thank Ute Goerke, Sahar Jalal, Andras Nemes, and Omid Amili for help during the MRI measurements and discussion in the analysis of the results.

GRANTS

Funding for this work was provided by the National Science Foundation (CBET-1453538) and the National Institutes of Health (NHLBI-R21HL129906). COPDGene was supported by Award Number R01 HL089897 and Award Number R01 HL089856 from the National Heart, Lung, and Blood Institute and by the COPD Foundation through contributions made to an Industry Advisory Board comprised of AstraZeneca, Boehringer Ingelheim, GlaxoSmithKline, Novartis, Pfizer, Siemens and Sunovion.

AUTHOR CONTRIBUTIONS

Author contributions: C.W. and F.C conception and design of research; T.V.M. and F.C. performed experiments; T.V.M. analyzed data; T.V.M., C.W. and F.C interpreted results of experiments; T.V.M. prepared figures; T.V.M. and F.C. drafted manuscript; T.V.M. and F.C. and C.W. edited and revised manuscript; F.C. approved final version of manuscript.

REFERENCES

1. Aysola RS et al. (2008) Airway Remodeling Measured by Multidetector CT Is Increased in Severe Asthma and Correlates With Pathology. Chest Journal 134(6):1183-1191
2. Banko AJ et al. (2015) Three-dimensional inspiratory flow in the upper and central human airways. Exp Fluids 56(6):1–12
3. Banko, A. J., Coletti, F., Elkins, C. J., & Eaton, J. K. (2016). Oscillatory flow in the human airways from the mouth through several bronchial generations. International Journal of Heat and Fluid Flow, 61, 45-57.
4. Boser SR et al. (2005) Fractal geometry of airway remodeling in human asthma. American journal of respiratory and critical care medicine, 172(7):817-823.
5. Boxt LM et al. (1994). Fractal analysis of pulmonary arteries: the fractal dimension is lower in pulmonary hypertension. Journal of thoracic imaging, 9(1): 8-13
6. Comer JK et al. (2001) Flow structures and particle deposition patterns in double-bifurcation airway models. Part 1. Air flow fields. J Fluid Mech 435:25–54
7. De Backer JW et al. (2008). Flow analyses in the lower airways: patient-specific model and boundary conditions. Medical engineering & physics, 30(7):872-879.
8. De Backer, J. W., Vos, W. G., Vinchurkar, S. C., Claes, R., Drollmann, A., Wulfrank, D., ... & De Backer, W. (2010). Validation of computational fluid dynamics in CT-based airway models with SPECT/CT. Radiology, 257(3), 854-862.
9. de Rochefort, L et al (2007). *In vitro* validation of CFD simulation in human proximal airways reconstructed from medical images with hyperpolarized helium-3 MRI phase contrast velocimetry. J. Appli. Physiol, 102(5):2012-2023.
10. de Vasconcelos TF et al (2011). Particle capture into the lung made simple? Journal of applied physiology, 110(6):1664-1673.

11. Elkins, C. J., Markl, M., Pelc, N., & Eaton, J. K. (2003). 4D Magnetic resonance velocimetry for mean velocity measurements in complex turbulent flows. Experiments in Fluids, 34(4), 494-503.
12. Elkins CJ et al. (2007). Magnetic resonance velocimetry: applications of magnetic resonance imaging in the measurement of fluid motion. Experiments in Fluids, 43(6):823-858.
13. Florens, M., Sapoval, B., & Filoche, M. (2011). An anatomical and functional model of the human tracheobronchial tree. Journal of Applied Physiology, 110(3), 756-763.
14. Fresconi FE & Prasad AK (2007). Secondary velocity fields in the conducting airways of the human lung. Journal of biomechanical engineering, 129(5):722-732.
15. Glenny RW & Robertson HT (2011). Determinants of pulmonary blood flow distribution. Comprehensive physiology.
16. Goldberger AL & West BJ (1991). Chaos and order in the human body. MD computing: computers in medical practice, 9(1):25-34.
17. Große S et al. (2007). Time resolved analysis of steady and oscillating flow in the upper human airways. Experiments in fluids, 42(6):955-970.
18. Grotberg JB (1994). Pulmonary flow and transport phenomena. Annual Review of Fluid Mechanics, 26(1):529-571.
19. Grotberg JB (2001). Respiratory fluid mechanics and transport processes. Annual review of biomedical engineering, 3(1):421-457.
20. Hasegawa et al. (2006). Airflow limitation and airway dimensions in chronic obstructive pulmonary disease. American journal of respiratory and critical care medicine, 173(12):1309-1315.
21. Hoffman EA at al. (2003). Characterization of the interstitial lung diseases via density-based and texture-based analysis of computed tomography images of lung structure and function 1. Academic radiology, 10(10):1104-1118.
22. Hoffman, E. A., Clough, A. V., Christensen, G. E., Lin, C. L., McLennan, G., Reinhardt, J. M., ... & Wang, G. (2004). The comprehensive imaging-based analysis of the lung: A forum for team science1. Academic radiology, 11(12), 1370-1380.
23. Horsfield K & Cumming G (1967). Angles of branching and diameters of branches in the human bronchial tree. Bulletin of Mathematical Biology, 29(2):245-259.
24. Horsfield K & Cumming G (1968). Morphology of the bronchial tree in man. Journal of Applied Physiology, 24(3):373-383.
25. Horsfield, K., Dart, G., Olson, D. E., Filley, G. F., & Cumming, G. (1971). Models of the human bronchial tree. Journal of applied physiology, 31(2), 207-217.
26. Horsfield K & Thurlbeck A (1981). Relation between diameter and flow in branches of the bronchial tree. Bulletin of mathematical biology, 43(6):681-691.
27. Horsfield K. (1985). Anatomical factors influencing gas mixing and distribution. Lung biology in health and disease, 25, 23-61.
28. Isabey D & Chang HK (1982). A model study of flow dynamics in human central airways. Part II: Secondary flow velocities. Respiration physiology, 49(1):97-113.
29. Jalal S et al. (2016). Three-dimensional inspiratory flow in a double bifurcation airway model. Experiments in Fluids, 57(9):148.
30. Jan DL et al. (1989). Some features of oscillatory flow in a model bifurcation. Journal of Applied Physiology, 67(1):147-159.

31. Kamiya A & Takahashi T (2007). Quantitative assessments of morphological and functional properties of biological trees based on their fractal nature. Journal of Applied Physiology, 102(6):2315-2323.
32. Kamm RD (1999). Airway wall mechanics. Annual review of biomedical engineering, 1(1):47-72.
33. Kassab GS (2006). Scaling laws of vascular trees: of form and function. American Journal of Physiology-Heart and Circulatory Physiology, 290(2):H894-H903.
34. Kim, Y., Sinclair, R., Chindapol, N., Kaandorp, J. A., & De Schutter, E. (2012). Geometric theory predicts bifurcations in minimal wiring cost trees in biology are flat. PLoS Comput Biol, 8(4), e1002474.
35. Kitaoka H & Suki B (1997). Branching design of the bronchial tree based on a diameter-flow relationship. Journal of Applied Physiology, 82(3):968-976.
36. Kitaoka H et al. (1999). A three-dimensional model of the human airway tree. Journal of Applied Physiology, 87(6):2207-2217.
37. Kleinstreuer, C., Zhang, Z., & Li, Z. (2008). Modeling airflow and particle transport/deposition in pulmonary airways. Respiratory physiology & neurobiology, 163(1), 128-138.
38. Kleinstreuer C. & Zhang Z (2010). Airflow and particle transport in the human respiratory system. Annual Review of Fluid Mechanics, 42:301-334.
39. Kleinstreuer, C., Zhang, Z., & Donohue, J. F. (2008). Targeted drug-aerosol delivery in the human respiratory system. Annu. Rev. Biomed. Eng., 10, 195-220.
40. Krause E et al. (1995). Fractal exponents for the upper airways of mammalian lungs. Computational Statistics & Data Analysis, 20(5):583-590.
41. Lambert AR et al. (2011). Regional deposition of particles in an image-based airway model: large-eddy simulation and left-right lung ventilation asymmetry. Aerosol Science and Technology, 45(1):11-25.
42. Lennon FE et al. (2015). Lung cancer - a fractal viewpoint. Nature Reviews Clinical Oncology, 12(11):664-675.
43. Lin CL et al. (2007). Characteristics of the turbulent laryngeal jet and its effect on airflow in the human intra-thoracic airways. Respiratory physiology & neurobiology, 157(2):295-309.
44. Ma B & Lutchen KR (2009). CFD simulation of aerosol deposition in an anatomically based human large–medium airway model. Annals of biomedical engineering, 37(2):271.
45. Majumdar A et al. (2005). Relating airway diameter distributions to regular branching asymmetry in the lung. Physical review letters, 95(16):168101.
46. Mandelbrot BB (1983). The Fractal Geometry of Nature. WH Freeman and Co.
47. Mandelbrot, B. (1990). Fractals-a geometry of nature. New Scientist, 127(1734), 38-43.
48. Markl M et al. (2012). 4D flow MRI. Journal of Magnetic Resonance Imaging, 36(5):1015-1036.
49. Martonen, T. B., Yang, Y., Hwang, D., & Fleming, J. S. (1995). Computer simulations of human lung structures for medical applications. Computers in biology and medicine, 25(5), 431-446.
50. Masters, B. R. (2004). Fractal analysis of the vascular tree in the human retina. Annu. Rev. Biomed. Eng., 6, 427-452.
51. Mauroy B et al. (2003). Interplay between geometry and flow distribution in an airway tree. Physical review letters, 90(14):148101.

52. Mauroy B (2004). An optimal bronchial tree may be dangerous. Nature, 427(6975):633-636.
53. Miyawaki, S., Hoffman, E. A., & Lin, C. L. (2016). Effect of static vs. dynamic imaging on particle transport in CT-based numerical models of human central airways. Journal of Aerosol Science, 100, 129-139.
54. Montaudon, M., Desbarats, P., Berger, P., De Dietrich, G., Marthan, R., & Laurent, F. (2007). Assessment of bronchial wall thickness and lumen diameter in human adults using multi-detector computed tomography: comparison with theoretical models. Journal of anatomy, 211(5), 579-588.
55. Murray CD (1926). The physiological principle of minimum work I. The vascular system and the cost of blood volume. Proceedings of the National Academy of Sciences, 12(3):207-214.
56. Nakano Y et al. (2000). Computed tomographic measurements of airway dimensions and emphysema in smokers: correlation with lung function. American journal of respiratory and critical care medicine, 162(3):1102-1108.
57. Nelson TR & Manchester DK (1988). Modeling of lung morphogenesis using fractal geometries. IEEE transactions on medical imaging, 7(4): 321-327.
58. Nelson TR et al. (1990). The fractal lung: universal and species-related scaling patterns. Cellular and Molecular Life Sciences, 46(3):251-254.
59. Nowak N et al. (2003). Computational fluid dynamics simulation of airflow and aerosol deposition in human lungs. Annals of biomedical engineering, 31(4):374-390.
60. Pedley TJ (1977) Pulmonary Fluid Dynamics. Annu Rev Fluid Mech 9(1):229-274
61. Pelc NJ et al. (1991). Encoding strategies for three□direction phase□contrast MR imaging of flow. Journal of Magnetic Resonance Imaging, 1(4):405-413.
62. Pelc NJ et al. (1994). Quantitative magnetic resonance flow imaging. Magnetic resonance quarterly, 10(3):125-147.
63. Phalen RF et al. (1978). Application of an idealized model to morphometry of the mammalian tracheobronchial tree. The Anatomical Record, 190(2):167-176.
64. Phillips CG & Kaye SR (1995). Diameter-based analysis of the branching geometry of four mammalian bronchial trees. Respiration physiology, 102(2-3):303-316.
65. Qian H & Bassingthwaighte JB (2000). A class of flow bifurcation models with lognormal distribution and fractal dispersion. Journal of theoretical Biology, 205(2):261-268.
66. Raabe OG et al. (1976). Tracheobronchial geometry: human, dog, rat, hamster.
67. Regan EA et al. (2011). Genetic epidemiology of COPD (COPDGene) study design. COPD: Journal of Chronic Obstructive Pulmonary Disease, 7(1):32-43.
68. Reynisson PJ et al. (2015). Airway Segmentation and Centerline Extraction from Thoracic CT–Comparison of a New Method to State of the Art Commercialized Methods. PloS one, 10(12).
69. Sauret V et al. (2002). Study of the three□dimensional geometry of the central conducting airways in man using computed tomographic (CT) images. Journal of anatomy, 200(2):123-134.
70. Schroter RC and Sudlow MF (1969). Flow patterns in models of the human bronchial airways. Respiration physiology, 7(3):341-355.
71. Soodt T et al. (2013). Analysis of basic flow regimes in a human airway model by stereo-scanning PIV. Experiments in fluids, 54(6).

72. Suwa N & Takahashi T (1971). Morphological and morphometrical analysis of circulation in hypertension and ischemic kidney. Urban & Schwarzenberg.
73. Tawhai MH & Lin CL (2011). Airway gas flow. Comprehensive Physiology, 1135–1157. John Wiley & Sons, Ltd.
74. Tawhai MH et al. (2004). CT-based geometry analysis and finite element models of the human and ovine bronchial tree. Journal of applied physiology, 97(6):2310-2321.
75. Thurlbeck A & Horsfield K (1980). Branching angles in the bronchial tree related to order of branching. Respiration physiology, 41(2):173-181.
76. Uylings HBM (1977). Optimization of diameters and bifurcation angles in lung and vascular tree structures. Bulletin of mathematical biology, 39(5):509-520.
77. Van Ertbruggen C et al. (2005). Anatomically based three-dimensional model of airways to simulate flow and particle transport using computational fluid dynamics. Journal of applied physiology, 98(3):970-980.
78. Wall WA & Rabczuk T (2008). Fluid–structure interaction in lower airways of CT-based lung geometries. International Journal for Numerical Methods in Fluids, 57(5):653-675.
79. Washko GR et al. (2014). Computed tomographic measures of airway morphology in smokers and never-smoking normals. Journal of applied physiology.
80. Weibel ER (1963) Principles and methods for the morphometric study of the lung and other organs. Lab Investig J Tech Methods Pathol 12:131
81. Weibel ER (1991). Fractal geometry: a design principle for living organisms. American Journal of Physiology-Lung Cellular and Molecular Physiology, 261(6): L361-L369.
82. Weibel ER (2009). What makes a good lung. Swiss Med Wkly, 139(27-28):375-386.
83. West GB et al. (1997). A general model for the origin of allometric scaling laws in biology. Science, 276(5309):122-126.
84. West BJ, Bhargava V, and Goldberger AL. "Beyond the principle of similitude: renormalization in the bronchial tree." Journal of Applied Physiology 60.3 (1986): 1089-1097.
85. Wilson TA (1969) Design of the bronchial tree. Nature 18, 668–669.
86. Xia G et al. (2010). Airway wall stiffening increases peak wall shear stress: a fluid–structure interaction study in rigid and compliant airways. Annals of biomedical engineering, 38(5):1836-1853.
87. Yin Y et al. (2010). Simulation of pulmonary air flow with a subject-specific boundary condition. Journal of biomechanics, 43(11):2159-2163.
88. Yin Y et al. (2013). A multiscale MDCT image-based breathing lung model with time-varying regional ventilation. Journal of computational physics, 244:168-192.
89. Zhang Z, Kleinstreuer C (2002) Transient airflow structures and particle transport in a sequentially branching lung airway model. Phys Fluids (1994-present) 14(2):862–880
90. Zhang, Z., Kleinstreuer, C., & Hyun, S. (2012). Size-change and deposition of conventional and composite cigarette smoke particles during inhalation in a subject-specific airway model. Journal of Aerosol Science, 46, 34-52.